Coupled optical and electronic simulations of electrically pumped photonic-crystal-based LEDs

Georgios Veronis[a], Yang Liu[a], Wonjoo Suh[a], Minghui Han[a], Zheng Wang[b], Robert W. Dutton[a], and Shanhui Fan[a]

[a]Department of Electrical Engineering, Stanford University, Stanford, California 94305;
[b]Department of Applied Physics, Stanford University, Stanford, California 94305

ABSTRACT

We use coupled optical and electronic simulations to investigate design tradeoffs in electrically pumped photonic crystal light emitting diodes. A finite-difference frequency-domain electromagnetic solver is used to calculate the spontaneous emission enhancement factor and the extraction efficiency as a function of frequency and of position of the emitting source. The calculated enhancement factor is fed into an electronic simulator, which solves the coupled continuity equations for electrons and holes and Poisson's equation. We simulate a two-dimensional structure consisting of a photonic-crystal slab with a single-defect cavity, and investigate different pumping configurations for such a cavity.

Keywords: Photonic crystal light emitting diode, electrically pumped device

1. INTRODUCTION

Recently, photonic crystals have shown the potential to dramatically improve the performance of several active optoelectronic devices, such as light emitting diodes (LEDs) and lasers. It has been suggested that a thin slab of two-dimensional photonic crystal in a LED can drastically enhance the light extraction efficiency.[1] The enhancement of light extraction in photonic crystal slabs has been verified in several experiments.[2–9] In addition, it has been shown both theoretically and experimentally that by introducing a single-defect on a two-dimensional photonic crystal slab, it is possible to obtain a wavelength-sized microcavity with a high quality factor Q. Such a small-volume high-Q cavity is a potential candidate for a thresholdless laser.[10–19]

Experimental efforts on photonic-crystal-based light emitting diodes and lasers are based on either optical pumping[2, 4, 5, 10, 11, 13–18] or electrical pumping.[3, 7–9, 12, 19] To realize electrically-pumped photonic-crystal optoelectronic devices, issues such as the device doping profile and placement of electrodes for carrier injection have to be addressed. In this work, we use two-dimensional coupled optical and electronic simulations to study theoretically different electrical pumping geometries. The simulated device consists of a photonic-crystal slab, which is the basis for most photonic-crystal active optoelectronic devices.[1, 4, 10, 11, 13–19] A defect is introduced in the photonic crystal to form a cavity. We examine several different configurations for pumping the device electrically. Carrier injection pipes are placed below the slab and electrodes are placed on top of the photonic-crystal grating. We investigate their effect on the light output of the cavity. We also investigate the effect of the doping profile.

This paper is organized as follows. The coupled optical and electronic simulation models are described in Section 2. The results obtained using these models for the various pumping configurations are presented in Section 3. Finally, our conclusions are summarized in Section 4.

2. MODEL DESCRIPTION

We solve the continuity equations for the electron and hole densities n and p, and Poisson's equation for the electrostatic potential ϕ over the device structure[20]:

$$\nabla \cdot \mathbf{j}_{\mathrm{n}} + U_{\mathrm{rad}}^{\mathrm{sp}} + U_{\mathrm{SRH}} + U_{\mathrm{Aug}} = 0 \tag{1}$$

$$\nabla \cdot \mathbf{j}_{\mathrm{p}} + U_{\mathrm{rad}}^{\mathrm{sp}} + U_{\mathrm{SRH}} + U_{\mathrm{Aug}} = 0 \tag{2}$$

$$-\nabla \cdot (\varepsilon \nabla \phi) + q(n - p - N_{\mathrm{D}}^{+} + N_{\mathrm{A}}^{-}) = 0 \tag{3}$$

Photonic Crystal Materials and Devices III, edited by Ali Adibi, Shawn-Yu Lin, Axel Scherer,
Proc. of SPIE Vol. 5733 (SPIE, Bellingham, WA, 2005) · 0277-786X/05/$15 · doi: 10.1117/12.590899

where N_D^+ and N_A^- are the densities of the ionized donors and acceptors, $\mathbf{j}_n$ and $\mathbf{j}_p$ are the electron and hole fluxes, and U_{rad}^{sp}, U_{SRH}, U_{Aug} are the rates for spontaneous emission (radiative recombination process), Shockley-Reed-Hall, and Auger recombination (nonradiative recombination processes) respectively. In the bulk regions of the device, carrier densities are calculated using Fermi-Dirac statistics, while in the quantum well region they are obtained based on a $\mathbf{k} \cdot \mathbf{p}$ band structure calculation.[21]

In the bulk region, nonradiative recombination processes are more important than spontaneous emission.[22] Thus, spontaneous emission in the bulk region is treated with the simple expression

$$U_{rad}^{sp} = B(np - n_0 p_0) \tag{4}$$

where B is the spontaneous emission coefficient and $n_0 p_0$ is the equilibrium product of electrons and holes. The spontaneous emission rate in the quantum well region is given by[22]

$$U_{rad}^{sp} = \int_0^\infty D(E) r^{sp}(E) dE \tag{5}$$

where $D(E)$ is the density of photon states, and $r^{sp}(E)$ is the spontaneous emission coefficient, which is determined by the $\mathbf{k} \cdot \mathbf{p}$ band structure calculation.

In the case of a uniform material, the density of photon states is given by[23]

$$D(E) = \frac{8\pi n_r^3 E^2}{h^3 c^3} \tag{6}$$

However, in photonic crystal devices, the density of photon states is strongly modified and can be either enhanced or suppressed with respect to the density in a uniform material.[24, 25]

The enhancement factor of the density of photon states due to the photonic crystal can be calculated using a classical electromagnetic model. The enhancement factor is equal to the ratio of the power radiated by a dipole in the presence of the device to the power radiated by the same dipole in a uniform material.[26] We use a finite-difference frequency-domain (FDFD) solver of Maxwell's equations[27] to calculate the spontaneous emission enhancement factor as a function of frequency and position of the emitting source. We note that frequency-domain techniques are much more efficient than time-domain techniques for such a calculation for the following reasons. First, the power emitted by a dipole at a specific frequency is obtained by integrating the Poynting vector over a surface surrounding the dipole. In the commonly-used finite-difference time-domain (FDTD) method the calculated fields on the surface have to be transformed to the frequency domain. However, this can only be done using a computationally expensive on-the-fly Fourier transform to avoid storing all the time samples of the fields over the entire surface. Second, FDFD results in a sparse system of linear equations. If a direct sparse matrix method is used to solve this system, only a single LU decomposition of the system matrix is required at each frequency. Once the LU decomposition of the system matrix is obtained, the only additional cost for the calculation of the enhancement factor for each different dipole position is one back-substitution, which is typically at least an order of magnitude smaller than the cost of the LU decomposition.

For emission from a quantum well we assume that the sources have horizontal orientation.[26] We use the FDFD method to calculate the photon density of states $D(E)$ as a function of position and frequency (or equivalently emitted photon energy). For each device geometry, $D(E)$ is precalculated and then fed into eq. (5) to calculate the spontaneous emission rate U_{rad}^{sp} in the quantum well region. The electronic equations (1)-(3) are then solved self-consistently using the general-purpose partial differential equation (PDE) solver Prophet.[28] The numerical implementation is based on finite-difference discretization of the PDEs and solution of the resulting nonlinear system of equations using Newton's method.

3. RESULTS

The device used in our simulations is a *p-i-n* structure shown in Fig. 1a. It consists of a single-quantum-well separate-confinement heterostructure (SCH).[23] The $Al_{0.3}Ga_{0.7}As$ SCH and the active region, consisting of an 80-Å GaAs QW, are undoped. This QW structure has a spontaneous emission spectrum with a maximum at

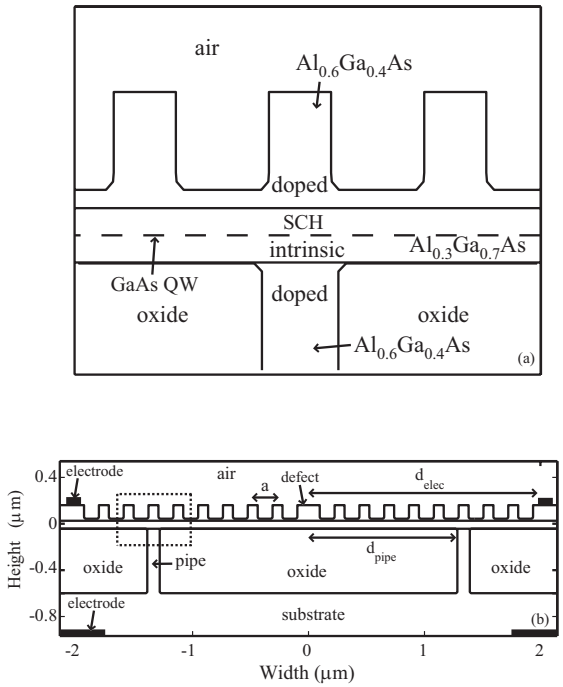

Figure 1. (a) The *p-i-n* device structure. The $Al_{0.3}Ga_{0.7}As$ separate-confinement heterostructure (SCH) and the active region, consisting of an 80-Å GaAs QW, are undoped. The SCH is surrounded by $Al_{0.6}Ga_{0.4}As$ doped to a density of 10^{18} cm^{-3} on both the p-side and the n-side. (b) The device geometry. The period of the grating is a=0.214μm. The reference device structure is characterized by $d_{\rm pipe}$=1.284μm and $d_{\rm elec}$=1.926μm. We also show with dashed lines the device area magnified in Fig. 1a.

$\sim$850 nm. The SCH is surrounded by $Al_{0.6}Ga_{0.4}As$ doped to a density of 10^{18} cm^{-3} on both the p-side and the n-side.

A cross-sectional view of the device geometry is shown in Fig. 1b. We assume that the device length is much larger than its height and width (Fig. 1b) and that the structure is uniform in the third dimension. We note that, even though we simulate a two-dimensional structure, the model takes into account both the radiation into free space in the vertical direction as well as the in-plane photonic bandgap. Thus, from an optical perspective, the model includes the essential physical characteristics of a more complicated photonic crystal slab structure. The device is based on a two-layer slab, consisting of the doped $Al_{0.6}Ga_{0.4}As$ upper cladding layer and the intrinsic $Al_{0.3}Ga_{0.7}As$ SCH layer, which also includes the active QW region. We use a low-index oxide as the bottom cladding layer of the slab to confine the optical mode. A one-dimensional photonic-crystal grating is introduced on the top of the slab. To minimize nonradiative surface recombination and to avoid degrading the QW, the grating does not penetrate into the intrinsic layer.[2] Using the MIT Photonic Band (MPB) package,[29] we design the photonic crystal grating to have a sizable photonic bandgap. We then introduce a single defect in the photonic crystal at the center of the device to create a resonant cavity. The defect width is chosen to obtain a cavity mode with the resonant frequency in the middle of the bandgap. In addition, the period of the grating is chosen as a=0.214μm, so that the resonant frequency coincides with the peak of the emission spectrum of the QW at $\sim$850nm. The number of periods of the photonic-crystal grating is chosen large enough to eliminate the in-plane leakage of light in the slab. We note that the quality factor Q of the cavity mode increases with the number of periods and eventually saturates, as it is limited by the out-of-plane leakage of light from the cavity. Since the bottom cladding layer is a low-index oxide, we introduce doped $Al_{0.6}Ga_{0.4}As$ pipes for carrier injection to obtain a complete *p-i-n* structure.[4, 13, 15, 18] We found that, if the pipe is placed directly below the cavity defect, the quality factor of the resonant mode decreases significantly. Pipes are therefore introduced laterally in the structure, as shown in Fig. 1b. The *p-i-n* structure is electrically pumped by placing electrodes on top of

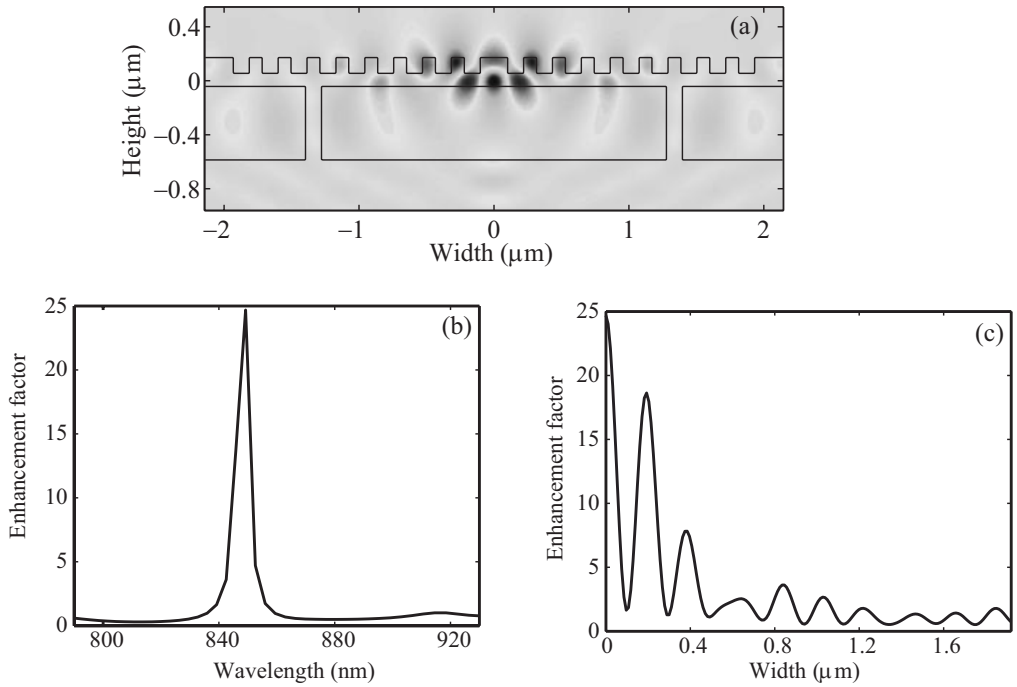

Figure 2. (a) The electric field profile when a dipole is placed in the QW at the center of the cavity defect and emitting at the resonant frequency of the cavity mode. (b) The calculated spontaneous emission enhancement factor as a function of wavelength for a dipole placed in the QW at the center of the cavity defect. (c) The calculated enhancement factor at the cavity resonant frequency as a function of emitter position in the QW.

the photonic crystal grating. In addition, the pipes are connected to a lower electrode through the $Al_{0.6}Ga_{0.4}As$ doped substrate (Fig. 1b). We found that the position of the lower electrode has no significant effect on the device electronics because the substrate is thick and highly doped. Since the device emits light primarily through the bottom, as mentioned below, the lower electrode is placed laterally to minimize the portion of reflected power.

In Fig. 2a, we show the electric field profile when a dipole is placed in the QW at the center of the cavity defect and emitting at the resonant frequency of the cavity mode. The photonic crystal confines the mode laterally so that in-plane light leakage in the slab is minimal. We also observe that out-of-plane leakage is much larger through the oxide cladding than through air, due to the smaller refractive index contrast between the slab and the oxide. Thus, the device emits light primarily through the bottom. In Fig. 2b, we show the calculated spontaneous emission enhancement factor as a function of wavelength for the dipole. Spontaneous emission is strongly enhanced within the cavity mode linewidth centered at ∼850 nm and suppressed in the bandgap off resonance.[30] In Fig. 2c, we show the enhancement factor at the cavity resonant frequency as a function of emitter position in the QW. As expected, this profile of the enhancement factor on resonance strongly correlates with the profile of the optical mode.

Our goal is to use the simulation model to investigate different electrical pumping configurations of the resonant cavity. More specifically, we study the effect of the position of the carrier injection pipes and of the upper electrodes deposited on top of the photonic crystal. Our standard reference device structure, shown in Fig. 1b, is characterized by d_{pipe}=1.284μm and d_{elec}=1.926μm, where d_{pipe} and d_{elec} are the distances of the pipes and upper electrodes respectively from the cavity center (Fig. 1b). In the following study, we vary either d_{pipe} or d_{elec} while keeping the other parameters the same as in the standard reference structure. We also study the effect of the doping configuration of the structure. We will refer to the doping configuration as P-i-N (N-i-P) if the upper cladding layer is P-doped (N-doped) and the carrier injection pipes and substrate are N-doped (P-doped).

In Figs. 3a and 3b, we show the electron density profile in the QW for the P-i-N and N-i-P configurations

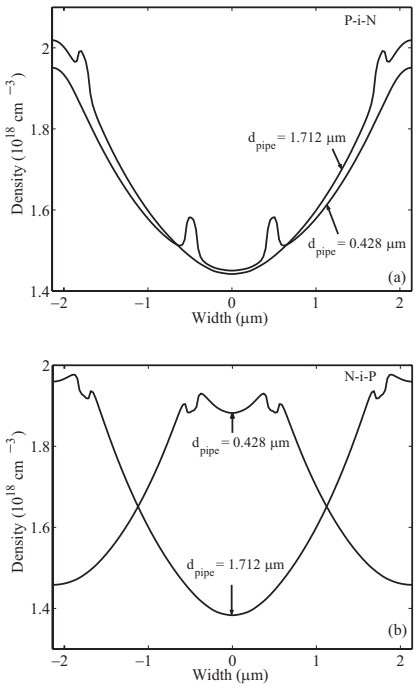

Figure 3. (a) The electron density profile in the QW for the P-i-N configuration. (b) The electron density profile in the QW for the N-i-P configuration. Results are shown for $d_{\rm pipe}$=0.428μm and $d_{\rm pipe}$=1.712μm. All other parameters are as in the reference structure (Fig. 1b).

respectively. Results are shown for $d_{\rm pipe}$=0.428μm and $d_{\rm pipe}$=1.712μm. We observe that in the P-i-N case, the carrier profile is almost insensitive to the pipes' position. Only the densities in the QW regions directly above the pipes are substantially different. On the contrary, in the N-i-P case the carrier profile is very sensitive to the position of the pipes. We found that this difference is due to the substantially lower hole mobility compared to electron mobility and consequently the lower hole diffusion coefficient. The diffusion of the charged carriers is primarily controlled by the slower species, i.e. the holes. In the N-i-P case the pipe positions directly affect the injection of holes, while in the P-i-N case they do not. We also found that, as expected, the opposite occurs if $d_{\rm elec}$ is varied instead of $d_{\rm pipe}$, i.e. the P-i-N configuration is sensitive to the variation of the position of the upper electrodes, while the N-i-P is not.

Since we are mainly interested in pumping the cavity resonance, we now focus our attention at the light generated in the QW through spontaneous emission at the resonant frequency and at the cavity center. As before, we examine alternative pumping configurations. In Figs. 4a, 4b (Figs. 4c, 4d), we show the electron and hole densities in the QW at the cavity center as a function of $d_{\rm pipe}$ ($d_{\rm elec}$). In addition, in Figs. 4a, 4c (4b, 4d), the doping configuration is P-i-N (N-i-P). The results are consistent with the discussion of Fig. 3. If $d_{\rm pipe}$ is varied in the P-i-N case, or $d_{\rm elec}$ in the N-i-P case the carrier concentrations are almost unaffected. On the contrary, carrier concentrations are substantially modified, if $d_{\rm pipe}$ is varied in the N-i-P case, or $d_{\rm elec}$ in the P-i-N case. More specifically, as $d_{\rm pipe}$ ($d_{\rm elec}$) increases in the N-i-P (P-i-N) case, the distance of the hole injection points from the cavity center increases and the carrier densities at the center therefore decrease. We also note that the imbalance of electron and hole densities in the QW is consistent with previous theoretical and experimental studies and in our case results from the asymmetric device geometry of the doped regions.[31,32]

In Fig. 5a (Fig. 5b), we show the spontaneous emission enhancement factor at the resonant frequency and at the cavity center in the QW as a function of $d_{\rm pipe}$ ($d_{\rm elec}$). We observe that in both cases the enhancement factor decreases as the distance from the cavity of either the pipes or the upper electrodes decreases. The energy of the optical resonant mode is concentrated in the vicinity of the defect region and decays away from it (Fig.

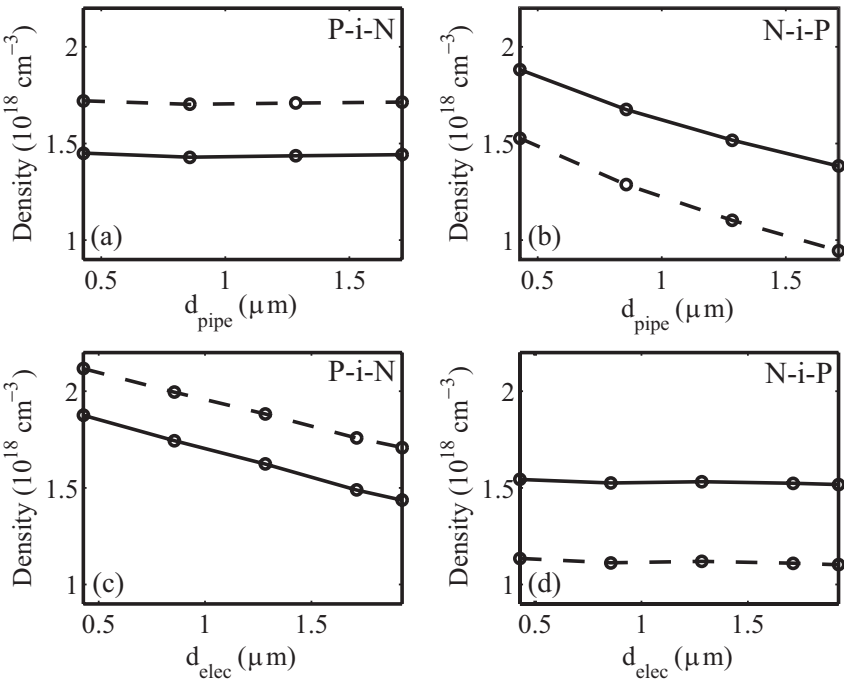

Figure 4. (a), (b) The electron and hole densities in the QW at the cavity center (Fig. 1b) as a function of $d_{\rm pipe}$. (c), (d) The electron and hole densities in the QW at the cavity center as a function of $d_{\rm elec}$. In Figs. 4a, 4c (4b, 4d), the doping configuration is P-i-N (N-i-P). Hole densities are shown with a dashed line. All other parameters are as in the reference structure (Fig. 1b).

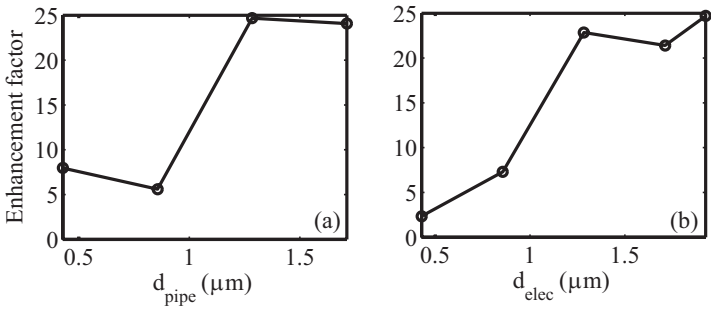

Figure 5. (a) The spontaneous emission enhancement factor at the resonant frequency and at the cavity center in the QW (Fig. 1b) as a function of $d_{\rm pipe}$. (b) The spontaneous emission enhancement factor at the resonant frequency and at the cavity center in the QW as a function of $d_{\rm elec}$. All other parameters are as in the reference structure (Fig. 1b).

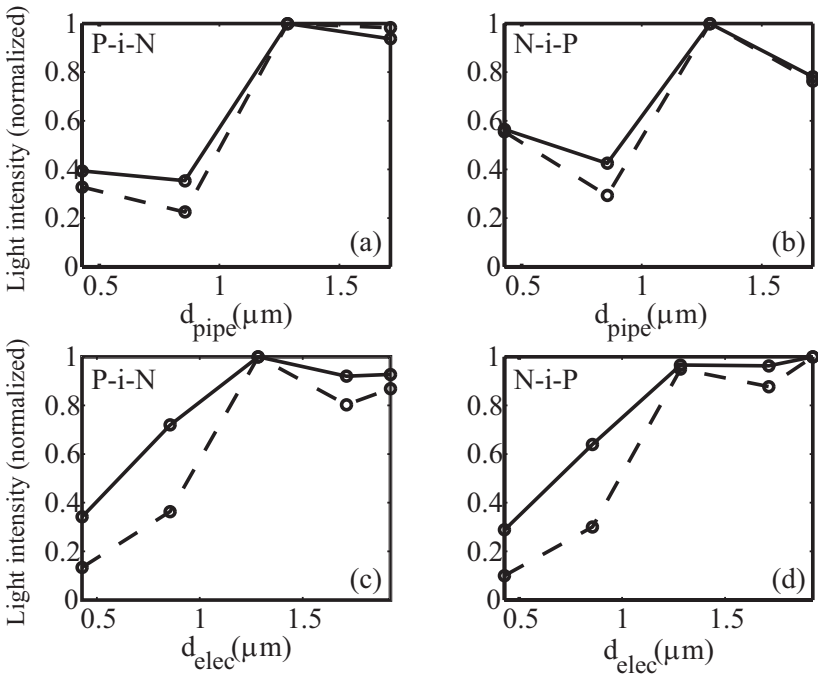

Figure 6. (a), (b) The light power generated in the QW at the cavity center (Fig. 1b) and at the resonance wavelength of ~ 850nm as a function of d_{pipe}. (c), (d) The light power generated in the QW at the cavity center and at the resonance wavelength as a function of d_{elec}. In Figs. 6a, 6c (6b, 6d), the doping configuration is P-i-N (N-i-P). We also show with a dashed line the product of the electron and hole densities at the cavity center and of the enhancement factor at the cavity center and at the resonance wavelength. All other parameters are as in the reference structure (Fig. 1b). All quantities are normalized with respect to their maximum value.

2). Thus, if the pipes or electrodes are placed at large distances from the device center, the optical mode and its quality factor Q are hardly affected. However, as the pipes or electrodes are placed closer to the device center they significantly affect the optical mode and decrease its Q. Thus, the enhancement of spontaneous emission on resonance also decreases.

In Fig. 6, we show the light power generated in the QW at the cavity center and at the resonance wavelength of ~ 850nm, as the pumping configuration is varied. We also show the product of the electron and hole densities at the cavity center and of the enhancement factor at the cavity center and at the resonance wavelength. We observe that these two quantities are strongly correlated but not identical. The difference between the two quantities is due to the fact that the spontaneous emission rate in the QW is determined from Eq. (5), in which the spontaneous emission coefficient $r^{\text{sp}}(E)$ is obtained from a $\mathbf{k} \cdot \mathbf{p}$ band structure calculation. On the other hand, the strong correlation between the two quantities suggests that the effect of device geometry on the light output of the cavity can be explained based on its effect on the carrier densities and on the optical resonant mode. Thus, we observe that, if the carrier densities are insensitive to device geometry modifications (as in Figs. 4a, 4d), the light output of the cavity is primarily determined by the enhancement factor (compare Fig. 5a with Fig. 6a, and Fig. 5b with Fig. 6d). In other cases, such as in Figs. 4b and 4c, there is a tradeoff between efficient carrier injection and high-quality-factor optical mode. Thus, in the cases of Figs. 4b and 4c, increasing the distance of either the electrodes or the pipes from the device center, increases the enhancement factor (Figs. 5a, 5b) but at the same time slightly decreases the carrier densities at the cavity (Figs. 4b, 4c). Due to such tradeoffs, there is an optimal pipe or electrode position for certain doping configurations, which maximizes the light output on resonance from the cavity (Figs. 6b, 6c).

The light output of the device depends on the generated optical power in the QW but also on the extraction efficiency of light. The photonic crystal grating on top of the device increases dramatically the extraction

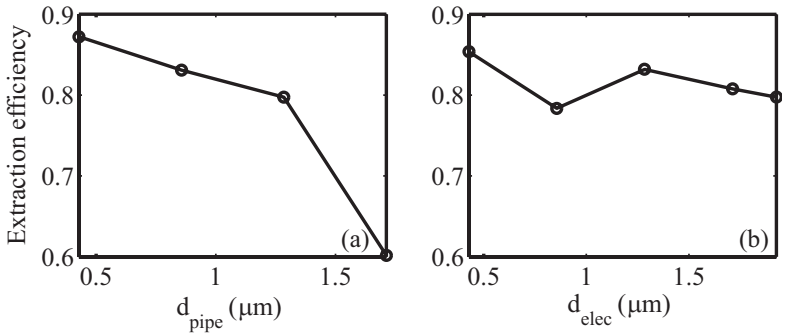

Figure 7. (a) The extraction efficiency at the resonant frequency and at the cavity center in the QW (Fig. 1b) as a function of d_{pipe}. (b) The extraction efficiency at the resonant frequency and at the cavity center in the QW as a function of d_{elec}. All other parameters are as in the reference structure (Fig. 1b).

efficiency of the device by eliminating the in-plane guided modes in the slab. As mentioned above, in-plane light leakage is minimal in the device of Fig. 1 and light is emitted primarily through the bottom (Fig. 2). We also investigate the effect of the pumping configuration on the extraction efficiency of the device, defined as the fraction of emitted flux through the top and bottom surfaces of the two-layer slab (Fig. 1) to the total emitted flux.[1] In Fig. 7a (Fig. 7b), we show the extraction efficiency, calculated with FDFD, for a dipole source at the resonant frequency and at the cavity center in the QW as a function of d_{pipe} (d_{elec}). We observe that the extraction efficiency increases as d_{pipe} decreases. If the pipes are placed closer to the device center, a portion of the emitted power is extracted through the pipes, thus increasing the extraction efficiency. However, as mentioned above, placing the pipes closer to the center substantially decreases the enhancement of spontaneous emission (Fig. 5a). On the contrary, d_{elec} has only a minimal effect on the extraction efficiency. The upper electrodes deposited on top of the grating cover only a small area of the device, so they do not reflect a significant portion of the emitted power. We also found that the fraction of extracted light power emitted through the bottom surface ranges from 88% to 94%, depending on the pumping configuration.

The pumping configuration has a significant effect on the light output of the cavity on resonance. Although the cavity defect can be designed to maximize the quality factor of the optical mode, the placement of pipes and electrodes for carrier injection may affect dramatically the light output of the cavity on resonance (Fig. 6). On the contrary, the total light output of the device over all wavelengths does not vary drastically with the pumping configuration. As an example, in Fig. 8 we show the total light output power extracted from the device as a function of the input electrical power for two different values of d_{pipe}. The difference between the two cases is small. We found that in general the pumping configuration does not significantly affect the overall light output of the device. Although spontaneous emission is substantially enhanced on resonance, it is suppressed off resonance, as mentioned above. We actually found that for any pumping configuration the enhancement factor averaged over all wavelengths and emitter positions is close to unity.

4. SUMMARY AND DISCUSSION

We used coupled optical and electronic simulations to model electrically-pumped photonic-crystal-based light emitting diodes. The FDFD method was used to calculate the spontaneous emission enhancement factor and the extraction efficiency. The calculated enhancement factor was fed into the electronic device equations which were solved self-consistently. We simulated a device consisting of a photonic-crystal slab with a single-defect cavity. Electrically, the device was a single-quantum-well *p-i-n* diode. The period of the photonic-crystal grating was chosen so that the resonant frequency of the cavity coincides with the peak of the emission spectrum of the QW at ∼850nm. We introduced doped pipes for carrier injection connected to a lower electrode through the substrate, and electrodes on top of the photonic crystal grating. We investigated the effect of the pipe and electrode position and of the doping configuration. We found that the pumping geometry can affect dramatically

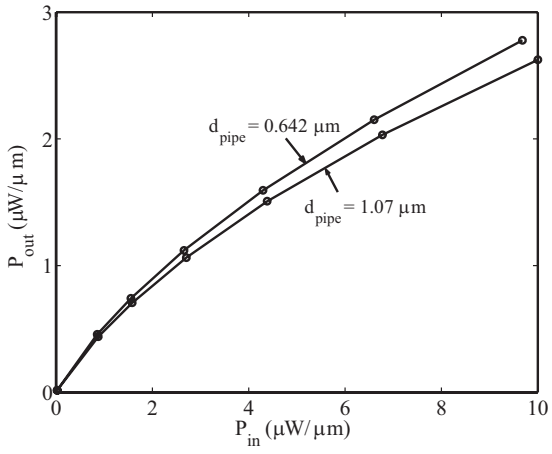

Figure 8. The total light output power per unit length extracted from the device as a function of the input electrical power per unit length for two different values of d_{pipe}. The doping configuration is P-i-N. All other parameters are as in the reference structure (Fig. 1b).

the light output of the cavity on resonance. The total light output of the device over all wavelengths has a weak dependence on the pumping configuration.

ACKNOWLEDGMENTS

This research was supported by DARPA/MARCO under the Interconnect Focus Center, and by the Center for Integrated Systems (CIS) at Stanford University.

REFERENCES

1. S. Fan, P. R. Villeneuve, J. D. Joannopoulos, and E. F. Schubert, "High extraction efficiency of spontaneous emission from slabs of photonic crystals," *Phys. Rev. Lett.* **78**, pp. 3294–3297, 1997.
2. A. A. Erchak, D. J. Ripin, S. Fan, P. Rakich, J. D. Joannopoulos, E. P. Ippen, G. S. Petrich, and L. A. Kolodziejski, "Enhanced coupling to vertical radiation using a two-dimensional photonic crystal in a semiconductor light-emitting diode," *Appl. Phys. Lett.* **78**, pp. 563–565, 2001.
3. H. Ichikawa and T. Baba, "Efficiency enhancement in a light-emitting diode with a two-dimensional surface grating photonic crystal," *Appl. Phys. Lett.* **84**, pp. 457–459, 2004.
4. H. Y. Ryu, J. K. Hwang, Y. J. Lee, and Y. H. Lee, "Enhancement of light extraction from two-dimensional photonic crystal slab structures," *IEEE J. Select. Topics Quantum Electron.* **8**, pp. 231–237, 2002.
5. T. Baba, K. Inoshita, H. Tanaka, J. Yonekura, M. Ariga, A. Matsutani, T. Miyamoto, F. Koyama, and K. Iga, "Strong enhancement of light extraction efficiency in GaInAsP 2-D-arranged microcolumns," *J. Lightwave Technol.* **17**, pp. 2113–2120, 1999.
6. B. J. Matterson, J. M. Lupton, A. F. Safonov, M. G. Salt, , W. L. Barnes, and I. D. W. Samuel, "Increased efficiency and controlled light output from a microstructured light-emitting diode," *Adv. Mater.* **13**, pp. 123–127, 2001.
7. M. Rattier, H. Benisty, R. P. Stanley, J. F. Carlin, R. Houdre, U. Oesterle, C. J. M. Smith, C. Weisbuch, and T. F. Krauss, "Toward ultrahigh-efficiency aluminum oxide microcavity light-emitting diodes: Guided mode extraction by photonic crystals," *IEEE J. Select. Topics Quantum Electron.* **8**, pp. 238–247, 2002.
8. T. N. Oder, K. H. Kim, J. Y. Lin, and H. X. Jiang, "III-nitride blue and ultraviolet photonic crystal light emitting diodes," *Appl. Phys. Lett.* **84**, pp. 466–468, 2004.
9. J. J. Wierer, M. R. Krames, J. E. Epler, N. F. Gardner, M. G. Craford, J. R. Wendt, J. A. Simmons, and M. M. Sigalas, "InGaN/GaN quantum-well heterostructure light-emitting diodes employing photonic crystal structures," *Appl. Phys. Lett.* **84**, pp. 3885–3887, 2004.

10. O. Painter, R. K. Lee, A. Scherer, A. Yariv, J. D. O'Brien, P. D. Dapkus, and I. Kim, "Two-dimensional photonic band-gap defect mode laser," *Science* **284**, pp. 1819–1821, 1999.
11. O. J. Painter, A. Husain, A. Scherer, J. D. O'Brien, I. Kim, and P. D. Dapkus, "Room temperature photonic crystal defect lasers at near-infrared wavelengths in InGaAsP," *J. Lightwave Technol.* **17**, pp. 2082–2088, 1999.
12. S. Noda, M. Yokoyama, M. Imada, A. Chutinan, and M. Mochizuki, "Polarization mode control of two-dimensional photonic crystal laser by unit cell structure design," *Science* **293**, pp. 1123–1125, 2001.
13. H. Y. Ryu, J. K. Hwang, and Y. H. Lee, "The smallest possible whispering-gallery-like mode in the square lattice photonic-crystal slab single-defect cavity," *IEEE J. Quantum Electron.* **39**, pp. 314–322, 2003.
14. H. Y. Ryu, H. G. Park, and Y. H. Lee, "Two-dimensional photonic crystal semiconductor lasers: Computational design, fabrication, and characterization," *IEEE J. Select. Topics Quantum Electron.* **8**, pp. 891–908, 2002.
15. H. G. Park, J. K. Hwang, J. Huh, H. Y. Ryu, S. H. Kim, J. S. Kim, and Y. H. Lee, "Characteristics of modified single-defect two-dimensional photonic crystal lasers," *IEEE J. Quantum Electron.* **38**, pp. 1353–1365, 2002.
16. J. K. Hwang, H. Y. Ryu, D. S. Song, I. Y. Han, H. K. Park, D. H. Jang, and Y. H. Lee, "Continuous room-temperature operation of optically pumped two-dimensional photonic crystal lasers at 1.6 μm," *IEEE Photon. Technol. Lett.* **12**, pp. 1295–1297, 2000.
17. J. K. Hwang, H. Y. Ryu, D. S. Song, I. Y. Han, H. W. Song, H. K. Park, Y. H. Lee, and D. H. Jang, "Room-temperature triangular-lattice two-dimensional photonic band gap lasers operating at 1.54 μm," *Appl. Phys. Lett.* **76**, pp. 2982–2984, 2000.
18. H. G. Park, S. K. Kim, S. H. Kwon, G. H. Kim, S. H. Kim, H. Y. Ryu, S. B. Kim, and Y. H. Lee, "Single-mode operation of two-dimensional photonic crystal laser with central post," *IEEE Photon. Technol. Lett.* **15**, pp. 1327–1329, 2003.
19. H. G. Park, S. H. Kim, S. H. Kwon, Y. G. Ju, J. K. Yang, J. H. Baek, S. B. Kim, and Y. H. Lee, "Electrically driven single-cell photonic crystal laser," *Science* **305**, pp. 1444–1447, 2004.
20. S. Selberherr, *Analysis and Simulation of Semiconductor Devices*, Springer-Verlag, Berlin, Germany, 1984.
21. D. Ahn, S. L. Chuang, and Y. C. Chang, "Valence-band mixing effects on the gain and the refractive index change of quantum-well lasers," *J. Appl. Phys.* **64**, pp. 4056–4064, 1988.
22. M. Grupen and K. Hess, "Simulation of carrier transport and nonlinearities in quantum-well laser diodes," *IEEE J. Quantum Electron.* **34**, pp. 120–140, 1998.
23. S. L. Chuang, *Physics of Optoelectronic Devices*, Wiley, New York, 1995.
24. E. Yablonovitch, "Inhibited spontaneous emission in solid-state physics and electronics," *Phys. Rev. Lett.* **58**, pp. 2059–2062, 1987.
25. S. John, "Strong localization of photons in certain disordered dielectric superlattices," *Phys. Rev. Lett.* **58**, pp. 2486–2489, 1987.
26. D. Delbeke, R. Bockstaele, P. Bienstman, R. Baets, and H. Benisty, "High-efficiency semiconductor resonant-cavity light-emitting diodes: A review," *IEEE J. Select. Topics Quantum Electron.* **8**, pp. 189–206, 2002.
27. S. D. Wu and E. N. Glytsis, "Finite-number-of-periods holographic gratings with finite-width incident beams: analysis using the finite-difference frequency-domain method," *J. Opt. Soc. Am. A* **19**, pp. 2018–2029, 2002.
28. C. Rafferty and R. K. Smith, "Making a prophet," *Comp. Model. Eng. Sci.* **1**, pp. 151–159, 2000.
29. S. G. Johnson and J. D. Joannopoulos, "Block-iterative frequency-domain methods for Maxwell's equations in a planewave basis," *Opt. Express* **8**, pp. 173–190, 2001.
30. E. F. Schubert, N. E. J. Hunt, M. Micovic, R. J. Malik, D. L. Sivco, A. Y. Cho, and G. J. Zydzik, "Highly efficient light-emitting diodes with microcavities," *Science* **265**, pp. 943–945, 1994.
31. G. A. Kosinovsky, M. Grupen, and K. Hess, "Effect of carrier charge imbalance on the threshold current in diode lasers with thin intrinsic quantum wells," *Appl. Phys. Lett.* **65**, pp. 3218–3220, 1994.
32. A. A. Chelny, M. S. Kobyakova, and P. G. Eliseev, "Effect of the doping level of a p-cladding layer on the performance of GaAs-AlGaAs multiquantum-well lasers," *IEEE J. Quantum Electron.* **40**, pp. 113–117, 2004.